

Theory of hot-carrier generation in bimetallic plasmonic catalysts

Hanwen Jin,[†] Matias Herran,[‡] Emiliano Cortés,[‡] and Johannes Lischner^{*,¶}

[†]*Department of Materials, Imperial College London, South Kensington Campus, London SW7 2AZ, UK*

[‡]*Nanoinstitute Munich, Faculty of Physics, Ludwigs-Maximilians-Universität München, 80539 Munich, Germany*

[¶]*Department of Materials and the Thomas Young Centre for Theory and Simulation of Materials, Imperial College London, South Kensington Campus, London SW7 2AZ, UK*

E-mail: j.lischner@imperial.ac.uk

Abstract

Bimetallic nanoreactors in which a plasmonic metal is used to funnel solar energy towards a catalytic metal have recently been studied experimentally, but a detailed theoretical understanding of these systems is lacking. Here, we present theoretical results of hot-carrier generation rates of different Au-Pd nanoarchitectures. In particular, we study spherical core-shell nanoparticles with a Au core and a Pd shell as well as antenna-reactor systems consisting of a large Au nanoparticle which acts as antenna and a smaller Pd satellite nanoparticle separated by a gap. In addition, we investigate an antenna-reactor system in which the satellite is a core-shell nanoparticle. Hot-carrier generation rates are obtained from an atomistic quantum-mechanical modelling technique which combines a solution of Maxwell's equation with a tight-binding description of the nanoparticle electronic structure. We find that antenna-reactor systems exhibit

significantly higher hot-carrier generation rates in the catalytic material than the core-shell system as a result of strong electric field enhancements associated with the gap between the antenna and the satellite. For these systems, we also study the dependence of hot-carrier generation rate on the size of the gap, the radius of the antenna nanoparticle and the direction of light polarization. Our insights pave the way towards a mechanistic understanding of hot-carrier generation in heterogeneous nanostructures for photocatalysis and other energy conversion applications.

Introduction

There is currently significant interest in harnessing energetic or "hot" electrons and holes generated in metallic nanoparticles for applications in photocatalysis¹⁻⁵, photovoltaics⁶⁻⁸ and sensing¹⁰⁻¹⁷. Metallic nanoparticles feature localized surface plasmons (LSPs) which give rise to large light absorption cross sections¹⁸. The LSP has a short lifetime (typically on the order of tens of femtoseconds). Among the various decay mechanisms, the Landau damping decay plays a prominent role because it results in the generation of hot carriers^{19,20}.

However, photocatalytic hot-carrier devices often have relatively low efficiencies²¹. A possible explanation for this is that standard plasmonic materials, such as Au and Ag, are generally not good catalysts²². Therefore, attempts have been made to combine plasmonic materials with catalytic materials, such as Pt, Pd or Rh, into functional nanoarchitectures. Examples of such heterostructures include Janus nanoparticles⁹, core-shell systems^{23,24} or nanoparticle dimers and trimers²⁵. Recently, Herran and coworkers studied different nanoarchitectures of Pd and Au, including core-shell nanoparticles and antenna-reactor systems in which a large Au nanoparticle is "decorated" with small Pd nanoparticles (or satellites), for the production of H₂ from formic acid²⁶. These authors found significant enhancements in H₂ production upon illumination of the plasmo-catalyst with the largest increase in chemical activity for antenna-reactor systems. Despite these advances, however, there is still no detailed mechanistic understanding of the catalytic activity in bimetallic nanoarchitectures²⁷.

Insights into microscopic hot-carrier processes, including their generation, thermalization and extraction, can be gained from theoretical modelling. Atomistic first-principles techniques, such as ab initio time-dependent density-functional theory, can be used to investigate hot-carrier processes in very small nanostructures²⁸, but are challenging to apply to experimentally relevant system sizes. On the other hand, non-atomistic approaches, such as jellium or spherical well models, can be applied to large systems, but do not capture important aspects, including d-band derived nanoparticle states or facet-specific surface properties^{40–46}. To address this challenge, Jin and coworkers recently developed a new approach that combines a solution of Maxwell’s equation with large-scale atomistic tight-binding models which enables the modelling of hot-carrier processes in nanoparticles containing millions of atoms³⁹. So far, however, this approach has only been applied to spherical nanoparticles.

In this paper, we use the method of Jin and coworkers³⁹ to study the enhancement hot-carrier generation in a catalytic metal (Pd) induced by the presence of a plasmonic metal (Au) in different bimetallic plasmo-catalytic nanoarchitectures. In particular, we study Au@Pd core-shell nanoparticles and antenna-reactor systems consisting of a large Au nanoparticle which acts as antenna and a small satellite nanoparticle. The satellite is either a spherical Pd nanoparticle or a Au@Pd core-shell nanoparticle. We compare our results to hot-carrier generation rates in spherical Pd nanoparticles. We find that the largest hot-carrier generation rates in the catalytic metal are found in antenna-reactor systems, in particular in those where the satellite nanoparticle is a core-shell system. This can be explained by the large enhancement of the electric field arising from the strongly confined plasmon mode associated with the gap between the antenna nanoparticle and the satellite nanoparticle. We also explore the dependence of hot-carrier generation rates on the light polarization, the size of the antenna nanoparticle and the gap size between the antenna nanoparticle and the satellite. The resulting insights pave the way towards a mechanistic design of heterogeneous nanoarchitectures for energy conversion devices. The approach can readily be applied to other materials.

Methods

Hot-carrier generation rates

We use the approach developed by Jin and coworkers³⁹ to calculate hot-carrier generation rates in Pd-Au nanoarchitectures. In this method, the rate of hot electrons $N_e(E, \omega)$ of energy E excited by light of frequency ω is obtained by evaluating Fermi's golden rule according to⁴⁰

$$N_e(E, \omega) = \frac{2}{V} \sum_{if} \Gamma_{if}(\omega) \delta(E - E_f; \sigma), \quad (1)$$

where i and f label the initial and final state with energy E_i and E_f , respectively. Also, V is the volume of the nanoparticle and we define $\delta(x; \sigma) = \frac{1}{\sqrt{2\pi\sigma^2}} \exp(-\frac{x^2}{2\sigma^2})$ with $\sigma = 0.05$ eV being standard deviation of the Gaussian. In the above, Γ_{if} is given by

$$\Gamma_{if}(\omega) = \frac{2\pi}{\hbar} \left| \langle f | \hat{\Phi}_{tot}(\omega) | i \rangle \right|^2 \delta(E_f - E_i - \hbar\omega; \gamma) f(E_i) (1 - f(E_f)), \quad (2)$$

where $f(E)$ is the Fermi-Dirac distribution with temperature $T = 298$ K, $\gamma = 0.06$ eV is a broadening parameter and $\hat{\Phi}_{tot}(\omega)$ denotes the total potential inside the nanoparticle. This potential is calculated using the quasistatic approximation³³⁻³⁸. In particular, we use the finite element method as implemented in COMSOL[®]⁴⁷ to solve the Laplace equation

$$\nabla \cdot (\epsilon(\mathbf{r}, \omega) \nabla \Phi_{tot}(\mathbf{r}, \omega)) = 0, \quad (3)$$

where $\epsilon(\mathbf{r}, \omega)$ is dielectric function of the material at position \mathbf{r} . We use experimental dielectric functions for Au⁴⁸ and Pd⁴⁸. In the calculations, we first specify the geometry of the nanoarchitecture and the external potential $\Phi_{ext}(\mathbf{r}, \omega) = -\mathbf{E}_0 \cdot \mathbf{r}$ with \mathbf{E}_0 denoting the corresponding electric field and then solve Laplace's equation subject to the far-field condition that

$$\lim_{|\mathbf{r}| \rightarrow \infty} \Phi_{tot}(\mathbf{r}, \omega) = \Phi_{ext}(\mathbf{r}, \omega). \quad (4)$$

Once the total potential of the full Au-Pd nanoarchitecture is determined, we evaluate the hot-carrier generation rate in the Pd subsystem (as only the hot carriers in the Pd are catalytically active). Note that our approach does not capture charge transfer processes between the Au and the Pd which can play an important role in core-shell nanoparticles^{30,31}. The electronic states of the Pd subsystem are obtained using the tight-binding method. For this, we first determine the atomic positions by carving the desired Pd shape (either a spherical nanoparticle or a spherical nanoshell) from the bulk material. The eigenstates of the Hamiltonian are expressed in terms of linear combinations of atomic orbitals according to $|i\rangle = \sum_{J,\alpha} C_{J,\alpha} |J, \alpha\rangle$, with J labelling atoms and α labelling orbitals. For each Pd atom, the basis consists of five 4d orbitals, one 5s orbital and three 5p orbitals. The hopping and onsite energies of the Pd tight-binding model are taken from the "Handbook of the Band Structures of Elemental Solids"²⁹.

The matrix element in Eq. 1 is evaluated using³²

$$\langle I, \alpha | \hat{\Phi}_{tot}(\omega) | J, \beta \rangle = \Phi_{tot}(\mathbf{r}_J, \omega) \delta_{I,J} \delta_{\alpha,\beta}, \quad (5)$$

where \mathbf{r}_J denotes the position of atom J and we have ignored the transition dipole contribution to the matrix elements (which we have found to be small in our previous calculations³⁹).

The total generation rate of hot carriers (both electrons and holes) per unit volume is given by

$$N_{tot}(\omega) = 2 \int_{E_F}^{\infty} N_e(E, \omega) dE \quad (6)$$

with E_F denoting the Fermi energy. The hot hole generation rate $N_h(E, \omega)$ is obtained by replacing E_f by E_i in Eq. 1.

Results

We have calculated hot-carrier generation rates in four systems, see Fig. 1: (a) spherical Pd nanoparticles consisting of 3589 atoms (corresponding to a diameter $D = 4.42$ nm), (b) spherical Au@Pd core-shell nanoparticles with a Au core (of diameter $D_c = 4.90$ nm) and a Pd shell (of thickness 0.40 nm containing 3740 Pd atoms), (c) a Au-Pd antenna-reactor architecture consisting of a small spherical Pd nanoparticle of the same size as in (a) which is separated by a small gap from a larger Au nanoparticle and (d) a Au-Au@Pd antenna-reactor architecture in which the small nanoparticle has a core-shell structure as in (b). The sizes of the Pd nanoparticle and of the Au@Pd core-shell nanoparticle are similar to the satellite nanoparticles used in the experiment of Herran and coworkers²⁶.

Figure 2(a) shows the evolution of the hot carrier generation rate for the spherical Pd nanoparticle as function of photon energy. Both the hot hole and the hot electron rates exhibit two peaks. The hot hole rate has a peak near the Fermi level with the hot electron rate having a corresponding peak at $\sim \hbar\omega$ above the Fermi level. The other peak of the hot hole rate is at $\sim -\hbar\omega$ and the hot electron rate has a corresponding peak just above the Fermi level. As the photon energy is varied, the peaks near the Fermi level are pinned at their positions, but the other peaks move to higher (in case of the hot electron rate) and lower (in case of the hot hole rate) energies. This finding can be understood from an analysis of the electronic structure of Pd. In particular, the band structure of Pd, see Fig. 1(e), exhibits flat d-bands just above and below the Fermi energy. These flat bands give rise to a large density of states which translates into a high hot carrier generation rate near the Fermi level. The positions of the other peaks are then determined by energy conservation, i.e. for each electron of energy E a corresponding hole of energy $E - \hbar\omega$ must be created. Finally, we do not observe a dramatic enhancement of the hot-carrier rates at a particular photon energy which reflects the absence of a strong LSP resonance in spherical Pd nanoparticles.

Figure 2(b) shows the dependence of the hot carrier generation rate of a Au@Pd core-shell nanoparticle on the photon energy. Again, the rates exhibit peaks near the Fermi level.

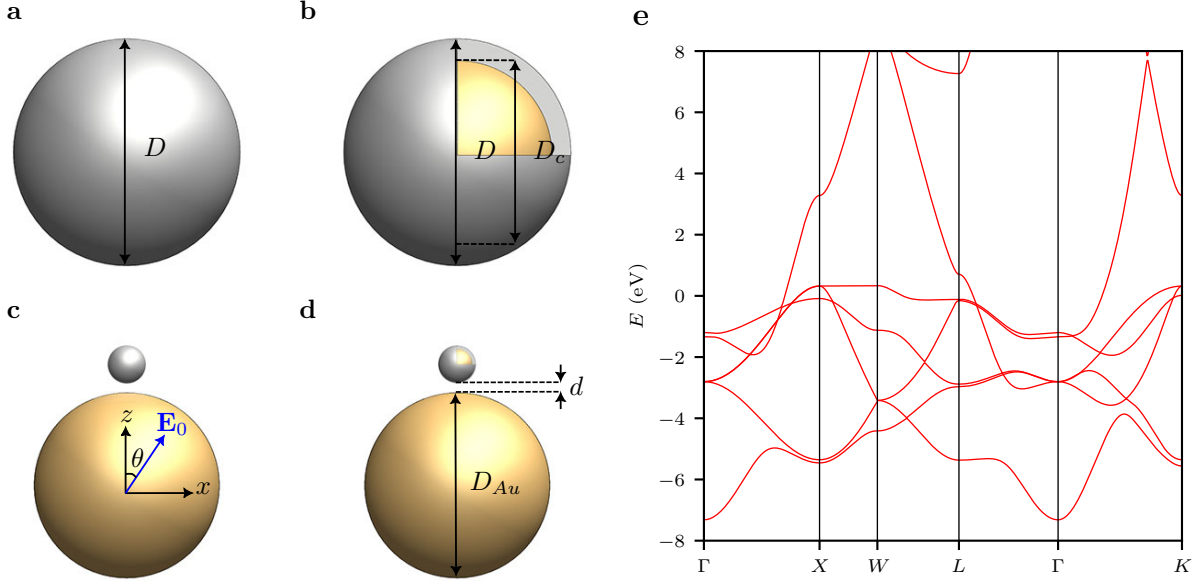


Figure 1: Schematic illustration of (a) a spherical Pd nanoparticle, (b) a Au@Pd core-shell nanoparticle, (c) a Au-Pd antenna-reactor system and (d) a Au-Au@Pd antenna-reactor system, (e) band structure of bulk fcc Pd, the zero of energy is set to the Fermi level.

Some differences in the shapes of the hot-carrier generation rates can be observed compared to the spherical Pd nanoparticle: these are caused by the increase of surface area of the thin Pd shell which enhances the generation of hot carriers from intraband transitions³⁹. In the core-shell system, an enhancement of the hot-carrier generation rate at a photon frequency of 2.4 eV can be observed. This energy is close to the LSP energy of a spherical Au nanoparticle. In other words, at this photon energy the field enhancement of the Au core increases the hot-carrier generation in the Pd shell³¹.

Next, we investigate hot-carrier generation in the Au-Pd antenna-reactor system. Adding the Au nanoparticle to the spherical Pd nanoparticle lifts the rotational symmetry of the Pd system. As a consequence, the hot-carrier generation rate now depends on the polarization vector of the electric field. We assume that both the centre of the Au and the centre of the Pd nanoparticle lie on the z -axis, see Fig. 1, and describe the electric field through its polar angle θ . Fig. 3(a) shows the dependence of the hot carrier rate on θ . The hot-carrier generation rate is largest when $\theta = 0^\circ$ and then decreases as θ is increased. In particular, we find that the

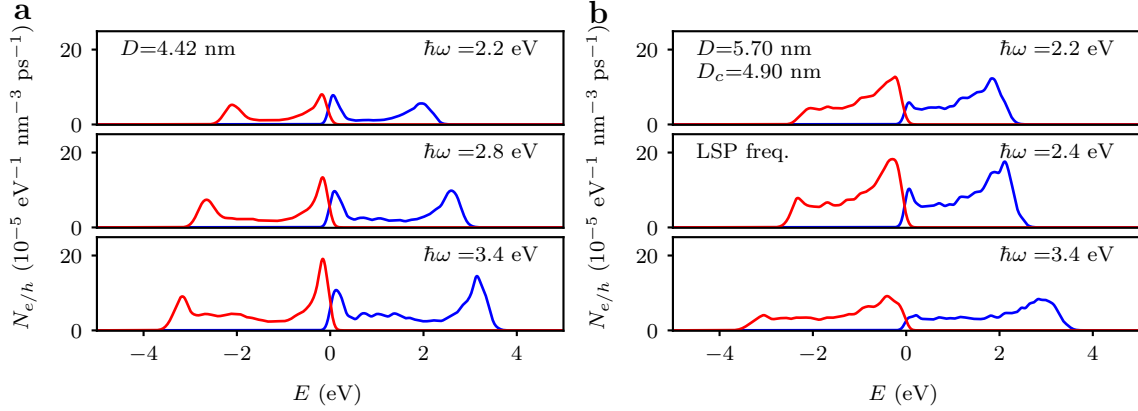


Figure 2: Dependence of hot-carrier generation rate on photon energy for (a) a spherical Pd nanoparticle with a diameter of $D = 4.42 \text{ nm}$ and (b) a Au@Pd core-shell nanoparticle with a core diameter of $D_c = 4.90 \text{ nm}$ and a shell thickness of 0.40 nm . Hot hole (electron) generation rates are red (blue). The zero of energy is set to the Fermi level.

hot-carrier generation rate is proportional to $\cos \theta$, i.e. $N_e(\omega, E, \theta) = N_e(\omega, E, 0) \cos \theta$. When $\theta = 0$, the charge carriers in the Au nanoparticle are pushed towards the Pd nanoparticle creating a strongly enhanced electric field. The field is further enhanced by the confinement effect of the small gap between between the Au and the Pd nanoparticles giving rise to a so-called gap plasmon⁴⁹. We note that a large number of satellites is attached to the Au nanoparticles in the experiments of Herran and coworkers²⁶. Also, the light used in experiments is not polarized. Therefore, the experimentally measured hot-carrier generation rate is an average over θ .

Figure 3 shows the same results for a Au-Au@Pd antenna-reactor system. Again, the hot-carrier generation rate of the core-shell system has a different shape than the pure Pd system, but it exhibits a similar dependence on the light polarization.

Next, we study the dependence of the hot-carrier generation rate of the two antenna-reactor systems on the size of the gap d between the Au nanoparticle and the satellite, see Fig. 4. In practice, this parameter is determined by the size of the ligands on the surface of the nanoparticles and is difficult to control experimentally (in the experiment of Herran et al., the gap is estimated to be approximately 1 nm ²⁶). We find that the largest hot-carrier rates are obtained for the systems with the smallest gaps. The insets show that the total

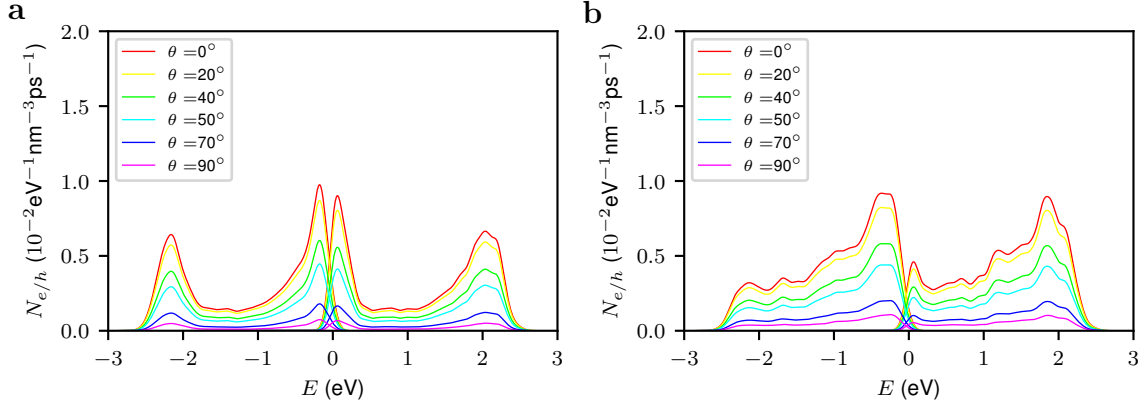


Figure 3: Dependence of hot-carrier generation rate on light polarization for (a) a Au-Pd antenna-reactor system with a diameter of 4.42 nm, (b) Au-Au@Pd reactor system, with a core diameter of 4.9 nm and a total diameter of 5.7 nm. The diameter of the Au nanoparticle is 49 nm. The size of the gap between the Pd and Au nanoparticles is 0.40 nm and the photon energy is 2.28 eV for Au-Pd system and 2.20 eV for Au-Au@Pd system.

number of hot carriers decreases quickly as the gap size is increased. For example, increasing the gap from 0.49 nm to 1.6 nm reduces the total number of hot carriers by a factor of 0.38 (Au-Au@Pd) and 0.42 (Au-Pd) and further increase to $d = 3.2$ nm gives rise to an additional reduction by a factor of 0.58 (Au-Au@Pd) and 0.63 (Au-Pd) in the total hot carrier generation rate. This result demonstrates the importance of the confinement effect associated with the gap between the Au and the satellite particles on the strength of the electric field.

Next, we study the dependence of the Pd hot-carrier generation rate of the reactor systems on the size of the Au nanoparticle, see Fig. 5. We find that the hot-carrier generation rate increases as the size of the Au nanoparticle increases. Increasing the Au nanoparticle size while keeping the distance between the Au nanoparticle and the satellite fixed reduces the volume available in the gap between the two nanoparticles and thus enhances confinement effects. This in turn leads to electric field enhancement. As the Au nanoparticle size increases, the additional reduction of the gap volume becomes less and less and only results in a small increase in hot carrier production.

Finally, we study the dependence of the hot-carrier generation rates of the reactor systems

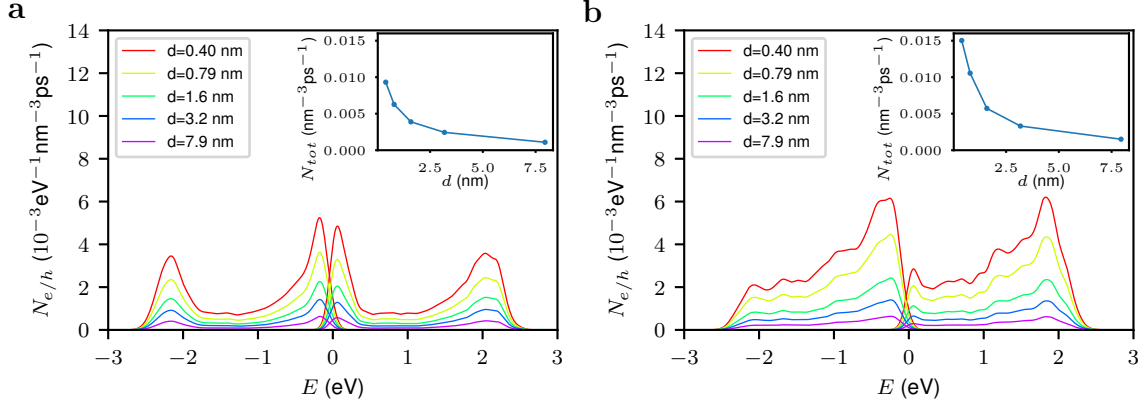


Figure 4: Dependence of the hot-carrier generation of Au-Pd antenna-reactor systems on the size of the gap d between the Au nanoparticle and the satellite. (a) Results for a Pd satellite. (b) Results for a Au@Pd core-shell satellite. The diameter of the Au antenna nanoparticle is 49 nm, the photon energy is 2.28 eV for Au-Pd system and 2.20 eV for Au-Au@Pd system and the calculation is averaged over all polarization angles. The insets show the total hot-carrier generation rate

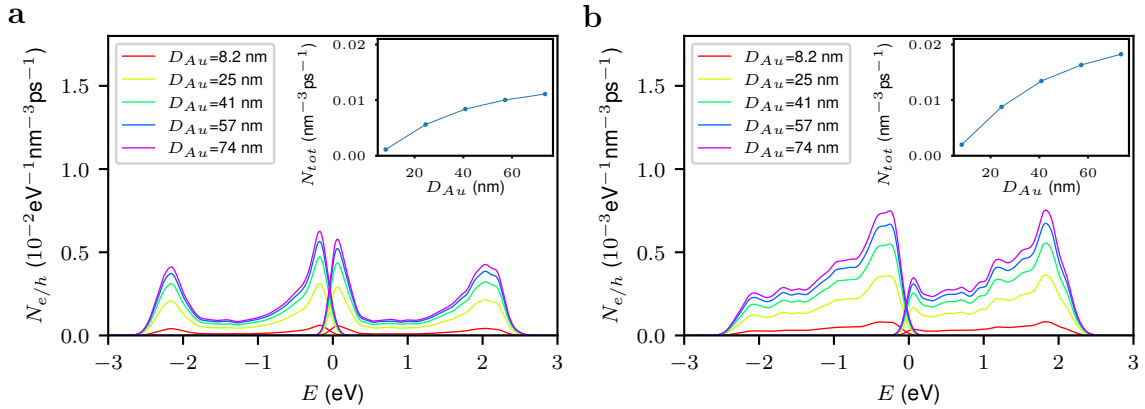


Figure 5: Dependence on the hot-carrier generation of Au-Pd antenna-reactor systems on the size of the Au nanoparticle. (a) Results for a Pd satellite. (b) Results for a Au@Pd core-shell satellite. The size of the gap is 0.40 nm, the photon energy is 2.28 eV for Au-Pd system and 2.20 eV for Au-Au@Pd system and the calculation was averaged over all polarization angles. The insets show the total hot-carrier generation rates.

on the photon energy, see Fig. 6. For both systems, a dramatic enhancements of the rates is observed at a photon energy of 2.24 eV compared to the other photon energies. This photon energy is close to the LSP energy of the Au nanoparticle (note that the presence of the satellite modifies the LSP energy of the Au nanoparticle) so the increase of the hot-carrier generation rates reflects the electric field enhancement caused by the plasmon mode. The LSP acts as an optical lens which efficiently funnels energy towards the catalytic material.

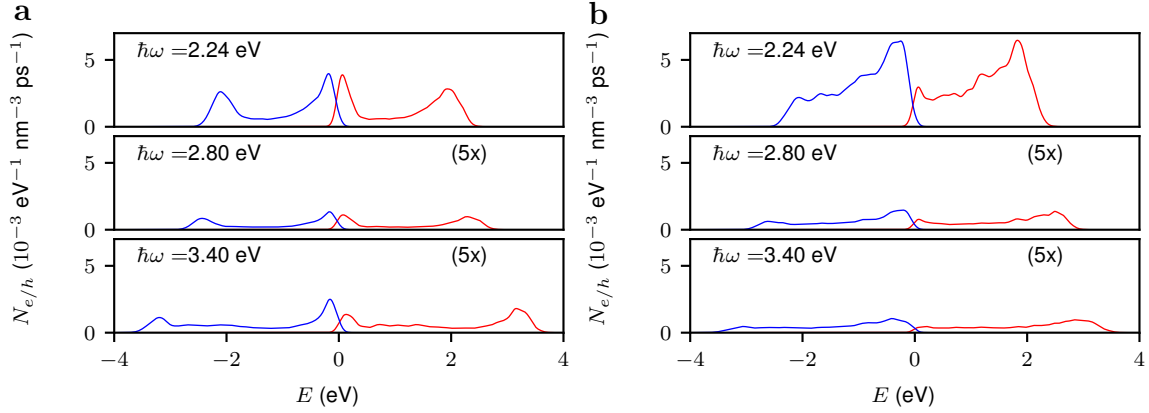


Figure 6: Dependence of hot-carrier generation rate on the photon energy for (a) a Au-Pd antenna-reactor system with a diameter of 4.42 nm, (b) Au-Au@Pd antenna-reactor system, with a core diameter of 4.9 nm and a total diameter of 5.7 nm. The diameter of the Au nanoparticle is 49 nm. The size of the gap between the Pd and Au nanoparticles is 0.40 nm, and the calculation is averaged over all polarisation angles. For visual aid, the hot-carrier generation rates at $\hbar\omega = 2.80$ eV and 3.40 eV were multiplied by a factor of 5.

We compare the total Pd hot-carrier generation rates of the 4 different systems (spherical Pd nanoparticle, Au@Pd core-shell nanoparticle, Au-Pd antenna-reactor system and Au-Au@Pd antenna-reactor system) in Fig. 7(a). It can be seen that the two antenna-reactor systems produce significantly more hot carriers in the Pd than the other two systems. In particular, a dramatic increase in the generation rate is observed near the plasmon frequency of ~ 2.2 eV. As discussed above, the large generation rates are a consequence of the gap plasmon mode, which gives rise to large electric field enhancements. In the antenna-reactor system with a core-shell satellite, the electric field is more strongly confined because of the presence of the Au inside the core-shell satellite and therefore this system gives rise to the largest hot-carrier generation rate overall.

In their experiments, Herran and coworkers measure the increase in H_2 production from formic acids by bimetallic plasmonic catalysts upon illumination with a solar simulator (see Figure 2(a) of Ref.²⁶). In Fig. 7(b) we show the measured difference in H_2 production in the dark and upon illumination for a Au@Pd core-shell nanoparticle, a Au-Pd antenna-satellite system and a Au-Au@Pd system. We compare this difference to the total number of hot holes N_{sol} generated by the solar spectrum $S(\omega)$ (using the Air Mass 1.5 spectrum) obtained via

$$N_{sol} = \int d\omega S(\omega) N_{tot}(\omega). \quad (7)$$

In excellent agreement with experiment, we find that the Au-Au@Pd antenna-satellite system is the best bimetallic plasmonic photocatalyst while the Au@Pd system performs much worse.

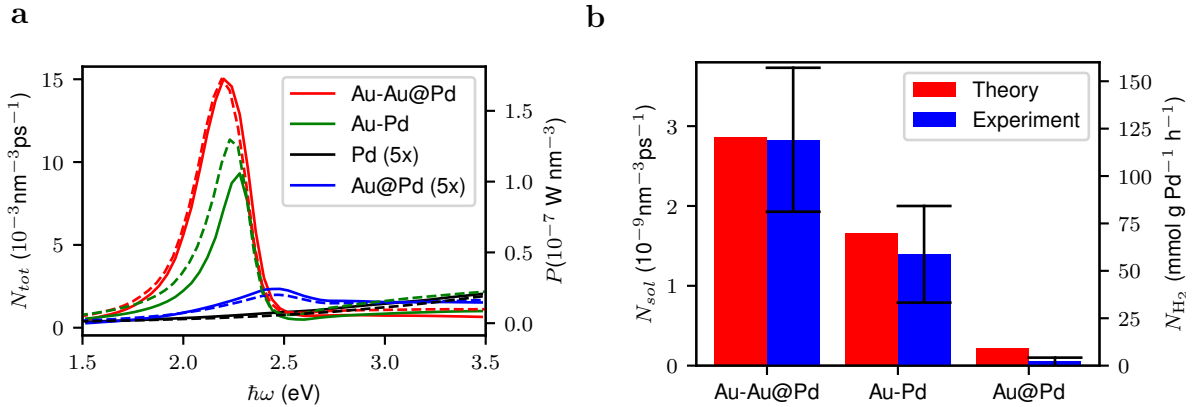


Figure 7: (a) Total hot carrier generation rate as a function of photon energy (averaged over all polarisation vectors) for a spherical Pd nanoparticle, a Au@Pd core-shell nanoparticle, a Au-Pd reactor and a Au-Au@Pd reactor. The power (per unit volume) absorbed by the Pd subsystem is shown in dashed lines. Note that the curves for the Pd nanoparticles and the Au@Pd have been multiplied by a factor of 5 to improve visibility. (b) Comparison of the measured difference in H_2 production upon illumination by a solar simulator and in the dark to the calculated number of hot holes excited by solar illumination.

Conclusion

We have studied hot-carrier generation in Au-Pd nanoarchitectures using an atomistic quantum-mechanical modelling approach. We have found that Au-Pd antenna-reactor systems exhibit significantly higher hot-carrier generation rates than core-shell nanoparticles. This is caused by the large electric field enhancements due to the localized plasmon mode associated with the gap between the antenna and the satellite nanoparticles. In particular, the largest overall hot-carrier generation rate is found for an antenna-reactor system in which the satellite is a core-shell nanoparticle. For the antenna-reactor systems, we also studied the dependence of the hot-carrier generation rates on the size of the gap, the radius of the antenna nanoparticle and the light polarization direction. We find that the largest rates are found when the electric field is parallel to the axis connecting the centres of the antenna and satellite nanoparticles. Also, small gaps and large antenna sizes favor hot-carrier generation. The insights from our work can guide the development of highly efficient heterogeneous hot-carrier nanodevices for energy conversion applications.

Acknowledgments

HJ acknowledges financial support from his parents. M.H. and E.C. acknowledge the Deutsche Forschungsgemeinschaft (DFG, German Research Foundation) under e-conversion Germany's Excellence Strategy – EXC 2089/1 – 390776260, the Bavarian program Solar Energies Go Hybrid (SolTech), the Center for NanoScience (CeNS) and the European Commission for the ERC-STG Catalight (802989). JL acknowledges funding from the EPSRC programme grant EP/W017075/1.

References

- (1) H. Robotjazi, H. Zhao, D. F. Swearer, N. J. Hogan, L. Zhou, A. Alabastri, M. J. McClain, P. Nordlander and N. J. Halas, Plasmon-induced selective carbon dioxide conversion on earth-abundant aluminum-cuprous oxide antenna-reactor nanoparticles, *Nat. Commun.* **8**, 27 (2017).
- (2) F. Mou, L. Xu, H. Ma, J. Guan, D. Chenb and S. Wang, Facile preparation of magnetic γ -Fe₂O₃/TiO₂ Janus hollow bowls with efficient visible-light photocatalytic activities by asymmetric shrinkage *Nanoscale* **4** 4650-4657 (2012)
- (3) Liu, XD., Chen, K., Ma, S. et al. Synthesis of Au/CdSe Janus Nanoparticles with Efficient Charge Transfer for Improving Photocatalytic Hydrogen Generation. *Nanoscale Res Lett* **14**, 349 (2019).
- (4) Y. Yuan, L. Zhou, H. Robotjazi, J. L. Bao, J. Zhou, A. Bayles, L. Yuan, M. Lou, M. Lou, S. Khatiwada, E. A. Carter, P. Nordlander, Earth-abundant photocatalyst for H₂ generation from NH₃ with light-emitting diode illumination *Science* **378**, 6622 (2022)
- (5) R. C. Elias , S. Linic, Elucidating the Roles of Local and Nonlocal Rate Enhancement Mechanisms in Plasmonic Catalysis *J. Am. Chem. Soc.* **144**, 43 (2022)
- (6) C. Clavero, Plasmon-Induced Hot-Electron Generation At Nanoparticle/Metal-Oxide Interfaces For Photovoltaic And Photocatalytic Devices, *Nat. Photonics* **8**, 95 (2014).
- (7) F. Enrichi, A. Quandt, and G. Righini, Plasmonic Enhanced Solar Cells: Summary Of Possible Strategies And Recent Results, *Renew. Sust. Energ. Rev.* **82**, 2433 (2018).
- (8) M. L. Salvador, B. A. MacLeod, A. Hess, A. P. Kulkarni, K. Munechika, J. I. L. Chen, and D. S. Ginger, Electron Accumulation On Metal Nanoparticles In Plasmon-Enhanced Organic Solar Cells, *ACS Nano* **6**, 10024 (2012).

- (9) A Chauhan, M. Rastogi , P. Scheier , C. Bowen , R. V. Kumar , R. Vaish, Appl. Phys. Rev. **5**, 041111 (2018).
- (10) I. Goykhman, B. Desiatov, J. Khurgin, J. Shappir, and U. Levy, Locally Oxidized Silicon Surface-Plasmon Schottky Detector For Telecom Regime, Nano Lett. **11**, 2219 (2011).
- (11) W. Li, and J. G. Valentine, Harvesting The Loss: Surface Plasmon-Based Hot Electron Photodetection, Nanophotonics **6**, 177 (2017).
- (12) H. Chalabi, D. Schoen, and M. L. Brongersma, Hot-Electron Photodetection With A Plasmonic Nanostripe Antenna, Nano Lett. **14**, 1374 (2014).
- (13) H. Tang, C. Chen, Z. Huang, J. Bright, G. Meng, R. Liu, and N. Wu, Plasmonic Hot Electrons For Sensing, Photodetection, And Solar Energy Applications: A Perspective, J. Chem. Phys. **152** , 220901 (2020).
- (14) Q. Sun, C. Zhang, W. Shao, and X. Li, Photodetection By Hot Electrons Or Hot Holes: A Comparable Study On Physics And Performances, ACS Omega **4**, 6020 (2019).
- (15) Y. Zhai, G. Chen, J. Ji, X. Ma, Z. Wu, Y. Li, and Q. Wang, Large-Scale, Broadband Absorber Based On Three-Dimensional Aluminum Nanospire Arrays Substrate For Surface Plasmon Induced Hot Electrons Photodetection, Nanotechnology **30**, 375201 (2019).
- (16) Y. Zhu, H. Xu, P. Yu, and Z. Wang, Engineering Plasmonic Hot Carrier Dynamics Toward Efficient Photodetection, Appl. Phys. Rev. **8**, 021305 (2021).
- (17) Aizpurua, Javier and Baletto, Francesca and Baumberg, Jeremy and Christopher, Phillip and De Nijs, Bart and Deshpande, Preeti and Fernandez, Yuri Diaz and Fabris, Laura and Freakley, Simon and Gawinkowski, Sylwester and others, Theory of hot electrons: general discussion, Faraday discussions 214, 245 (2019).

- (18) Stefan Maier, *Plasmonics fundamentals and applications*(2007), springer.
- (19) J. B. Khurgin, Hot carriers generated by plasmons: where are they generated and where do they go from there? *Faraday Discuss.* **214**, 35-58 (2019)
- (20) S. Link , M. A. El-Sayed, Spectral Properties and Relaxation Dynamics of Surface Plasmon Electronic Oscillations in Gold and Silver Nanodots and Nanorods. *J. Phys. Chem. B*, **103**, 40 (1999)
- (21) S. Ezendam, M. Herran, L. Nan, C. Gruber, Y. Kang, F. Gröbmeyer, R. Lin, J. Gargiulo, A. Sousa-Castillo, E. Cortés, Hybrid Plasmonic Nanomaterials for Hydrogen Generation and Carbon Dioxide Reduction, *ACS Energy Lett.* **7**, 2 (2022)
- (22) B. Hammer , J. K. Norskov , Why gold is the noblest of all the metals, *Nature* **376**, 238–240 (1995)
- (23) V. G. Rao, U. Aslam, S Linic, Chemical Requirement for Extracting Energetic Charge Carriers from Plasmonic Metal Nanoparticles to Perform Electron-Transfer Reactions, *J. Am. Chem. Soc.* **141**, 1 (2019)
- (24) S. Chavez, U. Aslam, S. Linic, Design Principles for Directing Energy and Energetic Charge Flow in Multicomponent Plasmonic, Nanostructures *J. Am. Chem. Soc.* **141**, 1 (2019)
- (25) N. Zohar, L. Chuntunov, G. Haran, The simplest plasmonic molecules: Metal nanoparticle dimers and trimers. *J. Photochem. Photobiol. C*, **21**, 26-39 (2014)
- (26) M. Herran, A. Sousa-Castillo, C. Fan, S. Lee, W. Xie, M. Döblinger, B. Auguie, E. Cortés, Tailoring Plasmonic Bimetallic Nanocatalysts Toward Sunlight-Driven H₂ Production *Adv. Funct. Mater.* **32**, 38 (2022).
- (27) C. Zhan , Q. Wang , J. Yi , L. Chen , D. Wu , Y. Wang , Z. Xie , M. Moskovits , Z.

- Tian, Plasmonic nanoreactors regulating selective oxidation by energetic electrons and nanoconfined thermal fields, *Sci. Adv.* , **7**, 10 (2021).
- (28) T. P. Rossi , P. Erhart, M. Kuisma, Hot-Carrier Generation In Plasmonic Nanoparticles: The Importance Of Atomic Structure, *ACS Nano* **14**, 9963 (2020).
- (29) D. Papaconstantopoulos, *Handbook of the band structure of elemental solids* (Springer, New York, 2015).
- (30) C. Engelbrekt, K. T. Crampton, D. A. Fishman, M. Law, V. Ara Apkarian, Efficient Plasmon-Mediated Energy Funneling to the Surface of Au@Pt Core–Shell Nanocrystals, *ACS Nano*, **14**, 4 (2020)
- (31) U. Aslam, S. Chavez , S. Linic, Controlling energy flow in multimetallic nanostructures for plasmonic catalysis, *Nature Nanotech* **12**, 1000–1005 (2017)
- (32) T. Pedersen, K. Pedersen, and T. B. Kriestensen, Optical Matrix Elements In Tight-Binding Calculations, *Phys. Rev. B* **63**, 201101 (2001).
- (33) M. Ruiz , O. Schnitzer. Plasmonic resonances of slender nanometallic rings, *Phys. Rev. B* **105**, 125412 (2022).
- (34) O. Schnitzer. Asymptotic approximations for the plasmon resonances of nearly touching spheres, *Eur. J. Appl. Math.* **31**, 246 (2019)
- (35) M. Ruiz, O. Schnitzer. Slender-body theory for plasmonic resonance, *Proc. R. Soc* **475**, 1471 (2019)
- (36) O. Schnitzer, V. Giannini, R. V. Craster, S. A. Maier. Asymptotics of surface-plasmon redshift saturation at subnanometric separations, *Phys. Rev. B* **93**, 041409 (2016).
- (37) O. Schnitzer. Singular perturbations approach to localized surface-plasmon resonance: Nearly touching metal nanospheres, *Phys. Rev. B* **92**, 235428 (2015)

- (38) C. Bohren, *Absorption and Scattering of Light by Small Particles*(1998), WILEY
- (39) H. Jin, M. Kahk, D. Papaconstantopoulos, A. Ferreira, J. Lischner , Plasmon-Induced Hot Carriers from Interband and Intraband Transitions in Large Noble Metal Nanoparticles, *PRX Energy* ,**1**, 1 (2022).
- (40) A. Manjavacas, J. G. Liu, V. Kulkarni, and P. Nordlander, Plasmon-induced hot carriers in metallic nanoparticles, *ACS nano*,**8**, 8 (2014).
- (41) L. R. Castellanos, O. Hess , J. Lischner. Single plasmon hot carrier generation in metallic nanoparticles *Commun Phys* **2**, 47 (2019)
- (42) L. Ranno, S. D. Forno , J. Lischner. Computational design of bimetallic core-shell nanoparticles for hot-carrier photocatalysis, *npj Comput Mater* **4**, 31 (2018).
- (43) S. D. Forno, L. Ranno, J. Lischner. Material, Size, and Environment Dependence of Plasmon-Induced Hot Carriers in Metallic Nanoparticles, *J. Phys. Chem. C* **122**, 15 (2018)
- (44) L. R. Castellanos, J. M. Kahk, O. Hess, J. Lischner. Generation of plasmonic hot carriers from d-bands in metallic nanoparticles *J. Chem. Phys.* **152**, 104111 (2020)
- (45) L. R. Castellanos, O. Hess, J. Lischner, Dielectric Engineering of Hot-Carrier Generation by Quantized Plasmons in Embedded Silver Nanoparticles, *J. Phys. Chem. C*, **125**, 5 (2021)
- (46) A. Govorov, H. Zhang, Y. Gun'ko, Theory of Photoinjection of Hot Plasmonic Carriers from Metal Nanostructures into Semiconductors and Surface Molecules, *J. Phys. Chem. C* **117**, 16616 (2013)
- (47) COMSOL Multiphysics[®] v. 6.1. www.comsol.com. COMSOL AB, Stockholm, Sweden.
- (48) H. William, *CRC handbook of chemistry and physics : a ready-reference book of chemical and physical data*, (CRC Press, Florida, 2015)

- (49) J. J. Baumberg, J. Aizpurua, M. H. Mikkelsen , D. R. Smith, Extreme nanophotonics from ultrathin metallic gaps, *Nat. Mater.* **18**, 668–678 (2019)